KeA1

CHINESE ROOTS
GLOBAL IMPACT

Contents lists available at ScienceDirect

Petroleum Science

journal homepage: www.keaipublishing.com/en/journals/petroleum-science



Original Paper

Correlating the carbonic acid reaction with tight sand and pure minerals during geological carbon storage



Yong-Peng Sun ^{a, b, *}, Guo-Liang Li ^b, Si-Zhe Zeng ^b, Jia-Wei Liu ^c, Xian-Fei Du ^d, Cai-Li Dai ^b

- ^a State Key Laboratory of Deep Oil and Gas, China University of Petroleum (East China), Qingdao, 266580, Shandong, China
- b School of Petroleum Engineering, China University of Petroleum (East China), Oingdao, 266580, Shandong, China
- ^c Shale Gas Research Institute of PetroChina, Southwest Oil & Gas Field Company, Chengdu, 610051, Sichuan, China
- ^d Changqing Oilfield, PetroChina, Xi'an, 124010, Shaanxi, China

ARTICLE INFO

Article history: Received 20 April 2024 Received in revised form 29 March 2025 Accepted 31 March 2025 Available online 1 April 2025

Edited by Yan-Hua Sun

Keywords: Carbonic acid—rock reaction CO₂ Reaction kinetics Tight sand Geological carbon storage

ABSTRACT

CO₂ injection into geological formations has been proven to be an effective approach for carbon storage. When dissolved in formation water, CO₂ forms carbonic acid that induces mineral dissolution at pore surfaces under acidic conditions. Comprehensive understanding of geochemical interaction between carbonic acid and reservoir rocks is crucial for assessing environmental impact on geological formations. This study focuses on a tight oil sandstone reservoir. After characterizing basic petrophysical properties and mineral composition of rock samples, a series of carbonic acid corrosion experiments with both core and corresponding pure mineral samples were carried out, respectively. Dissolution solutions collected during the experiments were analyzed to examine the variations of ion concentrations in both core and pure mineral solutions. The carbonic acid-pure mineral corrosion kinetics were investigated. The correlations between carbonic acid with core and pure mineral corrosion scenarios were established from the sample mass, reaction rate, and ion concentration. The results show that after corrosion, the mass of calcite and dolomite in the rock sample decreased by 66.7% and 27.3%, respectively. When the corrosion was stabilized, the concentrations of Ca^{2+} and Mg^{2+} in the core solution were 72.9 and 74.4 mg/L, respectively, which was 40.5-41.3 times higher than that of Na+. The reaction kinetics analysis of carbonic acid-rock revealed a two-stage reaction in the pure mineral corrosion process, rapid reaction stage, and slow reaction stage, with different reaction rate constants and reaction orders for each ion. With the correlation between carbonic acid reaction with core and pure minerals, an effective and rapid evaluation method with pure minerals for the carbonic water—rock reaction is established, which costs a shorter time and is easier to investigate. This study provides a simple and faster method to evaluate the carbonic acid corrosion reaction during geological carbon storage.

© 2025 The Authors. Publishing services by Elsevier B.V. on behalf of KeAi Communications Co. Ltd. This is an open access article under the CC BY-NC-ND license (http://creativecommons.org/licenses/by-nc-nd/

4.0/).

1. Introduction

CO₂ can be stored through geological methods, such as saline aquifer, oil and gas reservoir (Ozotta et al., 2021). CO₂ exhibits effective oil displacement in reservoirs, yielding economic benefits alongside carbon reduction (Cao et al., 2023). Currently, the share of unconventional reservoirs, notably tight and shale oil, in newly proven reserves is on a gradual rise (Zhao et al., 2023). Unlike conventional reservoirs, tight and shale reservoirs feature small pore throats (Liu et al., 2021). The primary method for developing

* Corresponding author.

E-mail address: sunyongpeng@upc.edu.cn (Y.-P. Sun).

tight reservoirs is through staged fracturing of long horizontal wells (Liu, 2022; Zou et al., 2021). However, rapid energy transfer and production decline occur after the fracturing process. CO₂ injection not only enhances formation capacity but also improves the recovery rate, offering significant potential applications (Wu et al., 2023; Yang et al., 2024; Cao et al., 2023; Li et al., 2023).

Upon CO₂ infiltration into the formation, it dissolved in the formation water, resulting in the formation of carbonic acid (Liang et al., 2021; Zhao et al., 2021; Zhou et al., 2021). Elevated temperatures and pressures enhance acidity, facilitating the dissolution of reservoir minerals. Elucidating the chemical reactions involving carbonic acid and minerals in the reservoir is crucial for a deeper comprehension of how carbonic acid—rock reactions affect

reservoir physical properties (Hematpur et al., 2023; Khather et al., 2022; Talebi et al., 2022; Xu et al., 2023; Yang et al., 2023). This insight serves as a theoretical foundation for applying CO₂ injection technology in the field to improve recovery efficiency in tight reservoirs (Yan et al., 2023).

CO₂ reacts with various types of rock minerals, and the reaction process is influenced by factors such as mineral type, reaction temperature, and reaction pressure (Fatah et al., 2021; Gholami and Raza, 2022; Liu et al., 2022; Song et al., 2020; Zhang et al., 2019). Scholars have employed laboratory experiments and numerical simulations to investigate the dissolution patterns over time of various types of minerals and rock samples under different temperature and pressure conditions, aiming to elucidate the carbonic acid—rock reaction process. Rock cores consist of various minerals in different proportions. Studying the reactions of different minerals with CO₂ is essential for understanding the phenomena of rock core reactions. Tang et al. (2006) conducted X-ray diffraction and energy-dispersive spectroscopy analyses on the chemical behavior of kaolinite in carbonic acid. In the 5% HCl + 7% HBF₄ system, the average corrosion rate was only 11.82%. Kaolinite exhibits relative stability in carbonic acid, primarily due to its formation in acidic media. Kaszuba et al. (2005) found that quartz surfaces were hardly dissolved when treated with CO2 under conditions of 200 °C and 20 MPa. Only a large amount of clay minerals covered the surface, indicating the good stability of quartz in CO₂ solutions. To clarify the influence of reaction status on corrosion extent. Zhou et al. (2016) studied the corrosion rates of rock fluids at 200 and 250 °C. They found that the dissolution of plagioclase was higher than that of potassium feldspar, and increasing temperature significantly increased dissolution rates. Under dynamic fluid-rock interactions, mineral dissolution was much higher than static fluid interactions, as flowing fluid could flush away dissolved minerals, facilitating further dissolution. In contrast, equilibrium was reached after 15 days in static fluid-rock interactions, but dynamic reactions did not reach equilibrium. To further understand the reaction conditions within rock cores, Sun et al. (2021) measured the changes in relative permeability of tight reservoirs before and after CO₂-carbonic acid corrosion using steady-state methods. They compared the mineralogical changes before and after rock dissolution, finding that corrosion between CO2 and minerals occurred in both small and large pores. With increasing reaction pressure, larger pores were more susceptible to expansion than smaller ones. Ferrodolomite, calcite, and dolomite were the most sensitive minerals, with dissolution rates exceeding 11.2 wt%. However, evaluating carbonic acid-rock reactions in porous media is time-consuming, and there are significant differences between pure mineral—carbonic acid reactions and porous media (Jia et al., 2022). The kinetics of carbonic acid reactions with tight rock cores and pure minerals under the same conditions are still unclear (Chen et al., 2023).

Currently, research on the interaction between CO_2 and rocks and minerals is predominantly within the realm of geochemistry (Li et al., 2022). Nevertheless, the assessment of dynamic carbonic acid—rock reactions in porous media is time-intensive (Eyinla et al., 2023; Liu et al., 2023; Lu et al., 2022; Memon et al., 2022; Wang et al., 2023), however, the pure mineral—carbonic acid experiment is time efficient. Nevertheless, there is a gap between the pure mineral—carbonic acid reactions and rock—carbonic acid reaction.

This study focuses on a representative tight sand oil reservoir. Initially, the mineral composition and content of the core are defined. Subsequently, distinct systems for carbonic acid—core mineral corrosion and carbonic acid—pure mineral corrosion are established. Corrosion experiments are conducted separately for both core and pure minerals. This process yields data on the mineral composition and ion concentration of the solution throughout

the dissolution. The kinetic equations for carbonic acid corrosion reactions with individual pure minerals are derived by fitting the parameters of the pure mineral corrosion reaction. Based on the mass, reaction rate, and ion concentration features of stable reactions between the core and pure mineral, a correlation method for the reaction between carbonic acid with the core and pure mineral is developed. Additionally, an evaluation method is established to assess the reaction between carbonic acid and pure mineral, enabling the evaluation of the dynamic carbonic acid—rock reaction during the carbon storage process in reservoir conditions.

2. Experimental

2.1. Materials

The core samples used in experiments were sandstone outcrop samples, which were acquired from the Changqing Oilfield. The core samples are 2.51 cm in diameter and 5.05 cm in length, respectively, with porosity of 11.25% and Klinkenberg permeability of $0.182\times10^{-3}~\mu\text{m}^2.$

The target reservoir depth ranges from 800 to 1850 m. The average reservoir temperature is 44 $^{\circ}$ C, and the formation pressure is 15 MPa

Ultrapure water used has a resistivity of 18.25 M $\Omega \cdot cm$ at 25 $^{\circ} C$ and pH of 7.

Natural pure mineral samples (purity > 95%), such as calcite, dolomite, potassium feldspar, albite, and ferrodolomite were also used for carbonic acid—pure mineral dissolution experiments, based on the XRD results of core samples taken from the target block. This approach aimed to establish a corrosion correlation with the results from core sample and pure minerals. These pure minerals were ground into powder with a particle size of 200—300 mesh using an agate mortar.

2.2. Experimental procedures

2.2.1. Carbonic acid-core corrosion experiment

- (1) A core cutting machine was used to slice the rock core into a 1.5 mm thickness samples. The ultrasonic cleaning machine was then employed to remove debris from the cutting surface. After dried in an oven, an X-ray diffractometer (D/ max250, Rigaku) was used for the mineral composition analysis. The remaining portion of the core was weighed for dry mass and then used in subsequent experiments.
- (2) A high-pressure core saturation instrument (BH-1, Hai'an Oil Scientific Instrument) was employed to vacuum the core for 12 h. Subsequently, the core was saturated with simulated formation water and pressurized at 20 MPa for 24 h.
- (3) The experimental setup, as shown in Fig. 1, was assembled. Initially, at room temperature, CO₂ was injected into the piston accumulator with the booster pump, reaching half of the predetermined pressure of 15 MPa (7.5 MPa). Subsequently, the temperature was elevated to the predetermined value of 44 °C. Once the pressure in the piston accumulator stabilized (consistently exceeding the preset value throughout the experiment), the exhaust valve was opened, and the pressure was reduced and stabilized to the preset value of 15 MPa. Then CO₂ was injected into the simulated formation water using the syringe pump (ISCO 260D, Teledyne) under a constant pressure of 15 MPa, ensuring complete CO₂ dissolution in the simulated formation water. Saturated carbonic acid was prepared when the flow rate of syringe pump stabilized at 0 mL/min.

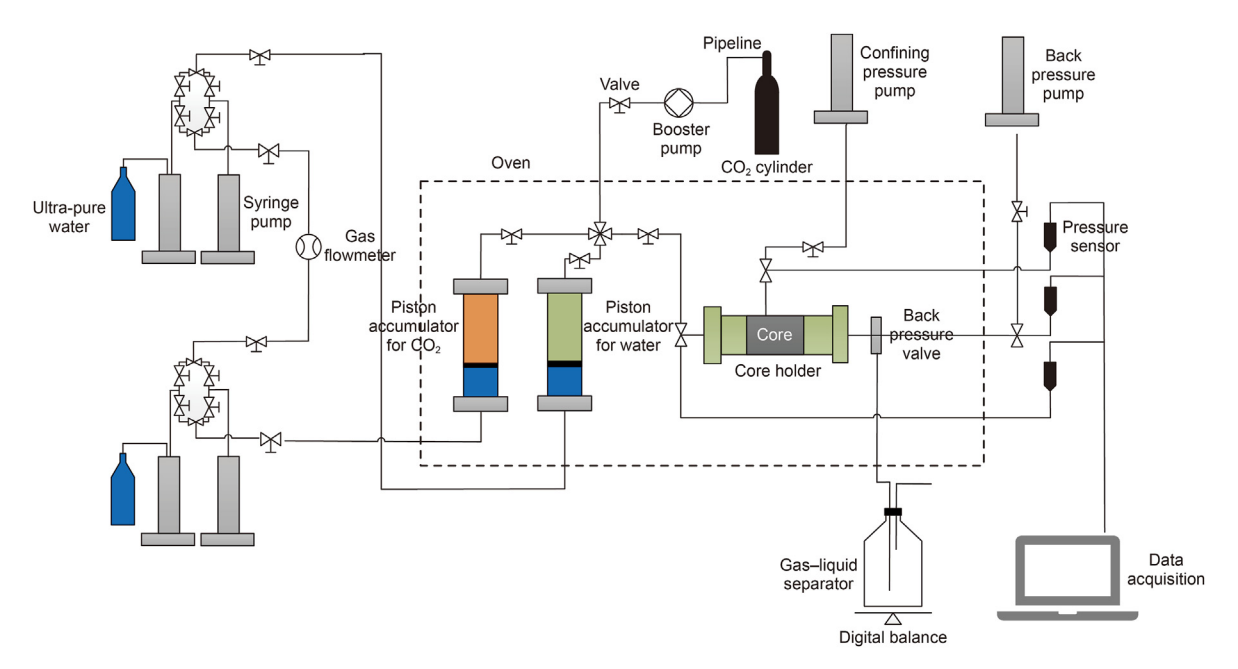


Fig. 1. Schematic diagram of carbonic acid—core corrosion experiment.

- (4) The water-saturated core was placed into the core holder and preheated for 2 h. The back-pressure pump was employed to elevate the pressure to the designated value of 15 MPa. A tracking pressure difference of 3 MPa was set at the confining pressure, to ensure that the confining pressure exceeded the injection pressure of 3 MPa consistently.
- (5) The syringe pump was utilized to introduce saturated carbonic acid into the core at a flow rate of 0.1 mL/min. Once the upstream pressure stabilized, a 10 h shut-in was carried out for the rock sample. Subsequently, saturated carbonic acid was reinjected into the core at a flow rate of 0.1 mL/min to achieve complete core dissolution. After the upstream pressure stabilized once again, the core displacement experiment was finished. Throughout the experiment, liquid samples were collected at 5, 10, 16, 20, 26, 39, 58, and 75 h, respectively, for ion analysis using an inductively coupled plasma mass spectrometer (ICPS-1000IV, Shimadzu).
- (6) After collecting the produced corrosion liquid, CO₂ was introduced into the core for drying, and the dissolved core was subsequently removed, dried, and weighed. A 1.5 mm thick slice was then cut from the inlet end, and core powder at the center of the slice was chosen for the mineral composition analysis.

2.2.2. Carbonic acid-pure mineral corrosion experiment

- (1) Four grams of pure minerals were weighted and subsequently dried and grounded into 200—300 mesh powder. Then the mineral powders were placed into a reagent bottle with 30 mL of ultra-pure water. Several holes were punctured through the reagent bottle cap to ensure the smooth entry of CO₂. Finally, the reagent bottle was placed into the piston accumulator.
- (2) The experimental device was assembled as per the configuration outlined in Fig. 2, then the aforementioned step (3) was repeated to establish a high-pressure CO₂ piston accumulator.

- (3) CO₂ was introduced into the piston accumulator at 15 MPa through a syringe pump, to make sure a continuous saturation of carbonic acid in the water within the reagent bottle. This saturated carbonic acid facilitated the complete corrosion of the mineral powder, initiated the corrosion reaction in the piston accumulator. Throughout the experiment, the injection of CO₂ into the piston accumulator was carried out using a syringe pump at a constant preset pressure.
- (4) A total of 5 sampling times were designated, 6, 30, 40, 52, and 75 h, respectively. Samples were extracted from the piston accumulator at each specified time. Once reached the sampling time, the inlet valve of the corresponding piston accumulator was closed to maintain constant pressure of the others. The pressure in the specific accumulator was released, the dissolution solution was collected. Ionic composition and content in the liquid were analyzed using the inductively coupled plasma mass spectrometer. Then the remaining powder in the reagent bottle was dried, and the dry mass was measured.
- (5) Upon completion of all sampling procedures, steps (1) to (3) were repeated with another pure mineral as outlined above.

In order to calculate the pH of carbonic acid in the experimental conditions, the dissolved volume of CO_2 in certain volume of water is needed. According to the injected volumes of CO_2 and water and the container pressure, the solubility of CO_2 is calculated to be 25.5 $\rm m^3/m^3$ at experimental conditions (44 °C and 15 MPa), which is equivalent to 25.5 L/L. Under standard conditions (0 °C, 0.1 MPa), the molar volume of CO_2 is 22.414 L/mol. At 44 °C and 15 MPa, we need to consider the equation of state for ideal gas to estimate the molar volume as Eq. (1):

$$V_{\rm m} = RT/P \tag{1}$$

where $V_{\rm m}$ is the molar volume, L/mol; R is the universal gas constant, L•MPa/(mol•K); T is temperature, K; P is pressure, MPa.

It is calculated that V_m is 0.1758 L/mol at 44 °C and 15 MPa. The molar concentration of CO_2 in solution is equal to 145.02 mol/L. The equation of CO_2 dissolved in water is as follows:

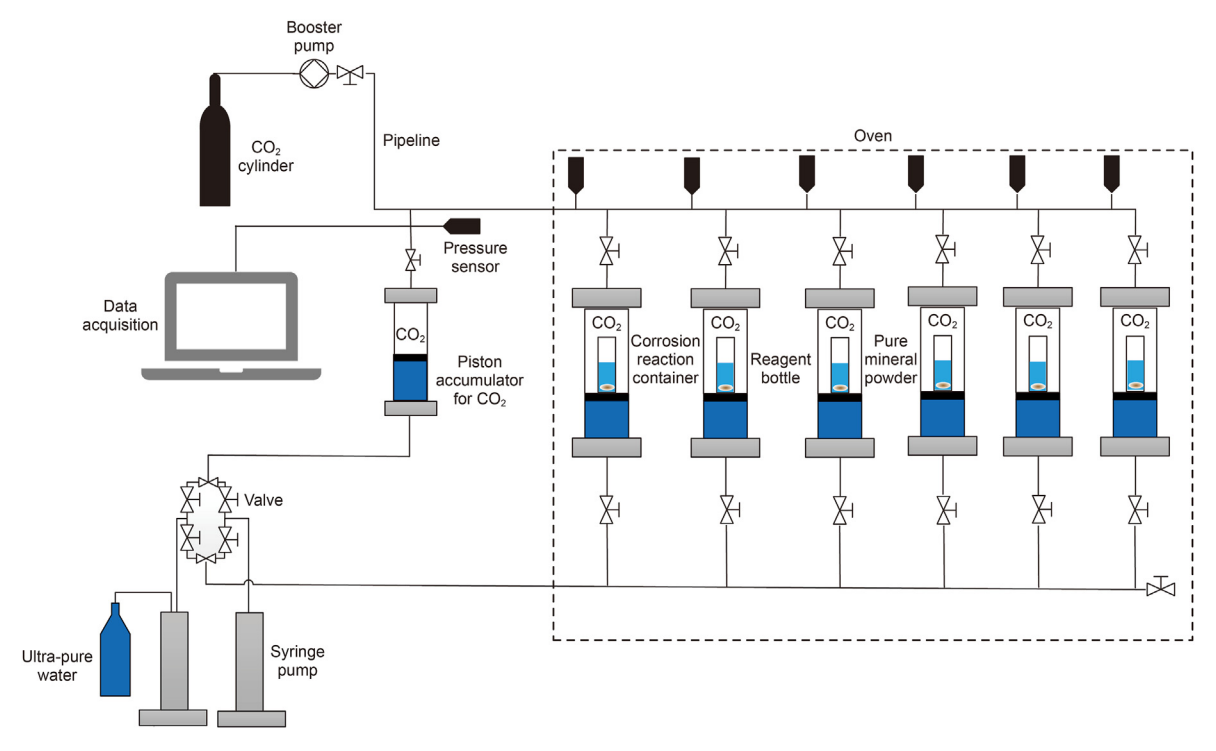


Fig. 2. Schematic diagram of carbonic acid—pure mineral corrosion experiment.

$$CO_2 + H_2O \leftrightarrow H_2CO_3$$

$$H_2CO_3 \leftrightarrow H^+ + HCO_3^-$$

We focus on the dissociation in the first step, where the equilibrium constant $K_a = 4.3 \times 10^{-7}$. Since only 0.3% of dissolved CO₂ formed H₂CO₃, the concentration of carbonic acid is 0.44 mol/L, $[H^+] = \sqrt{K_a \times [H_2CO_3]} = 4.34 \times 10^{-4}$, pH = $-\log[H^+] = 3.4$. Therefore, the theoretical pH of saturated carbonic acid under the experimental conditions is calculated to be 3.4, which is close to the similar experimental conditions from previous study (Wigand et al., 2008).

3. Results

3.1. Mineral variation during carbonic acid corrosion

3.1.1. Original mineral composition of core samples

The varied mineral composition of the core influences its interaction with CO₂. After the thin slice of the core was dried, the core powder was prepared using an agate mortar. Subsequently, the mineral composition of the core powder was analyzed with an XRD instrument (D/max250, Rigaku). The results are detailed in Fig. 3.

The core is predominantly composed of silicate and carbonate minerals. Quartz accounts for the largest proportion of 49%. The amount of minerals that could react with carbonic acid accounts for 48% of the total core minerals. Specifically, it contains 14% albite, 10% ferrodolomite, 11% dolomite, 10% potassium feldspar, and 3% calcite. The content of clay minerals is minimal, only 3%. This composition represents a typical tight sandstone formation with significant feldspar content.

3.1.2. Corrosion of core samples

Weighing the core mass before and after dissolution, we

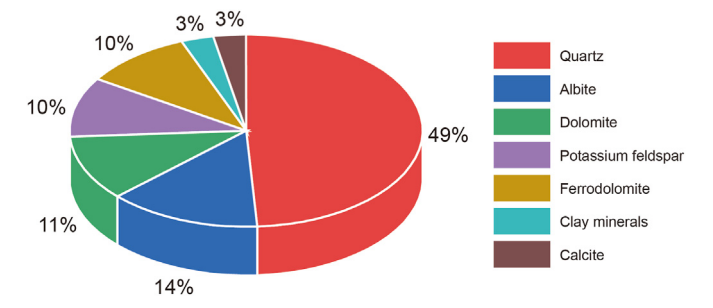


Fig. 3. Mineral composition of the outcrop core sample.

observed that the mass of the core before corrosion was 59.194~g, and after dissolution, it reduced to 58.469~g, representing a decrease of 1.22%. Based on the XRD results of the core before and after dissolution, the reaction equations for each mineral with CO_2 are provided in Table 1.

After the corrosion reaction, the relative contents of calcite, dolomite, potassium feldspar, albite, and ferrodolomite decrease by 66.7%, 27.3%, 20%, 14.3%, and 10%, respectively. Upon CO₂ injection into the reservoir, calcite, dolomite, potassium feldspar, albite, and ferrodolomite react with carbonic acid, forming soluble bicarbonate and leading to the dissolution of minerals in proximity to the pores. Consequently, the content of each mineral decreases, resulting in a decline in the core mass.

After the corrosion reaction, the quartz content in the core increased from 49% to 57%. Owing to the substantial feldspar content in the core, the corrosion reaction of potassium feldspar and albite with carbonic acid generates silicic acid. Due to the instability of silicic acid, it will lead to the decomposition of silicic acid into quartz. After the corrosion reaction, the content of clay minerals increased from 3% to 5%, primarily attributed to the elevated feldspar content in the core. Under experimental conditions, carbonate acid reacts with feldspar and produces precipitation of kaolinite.

Table 1
Chemical reactions between minerals and carbonic acid.

Mineral	Reaction equation	Produced mineral
Calcite (CaCO ₃) Dolomite (CaMg(CO ₃) ₂) Potassium feldspar (KAlSi ₃ O ₈) Albite (NaAlSi ₃ O ₈) Ferrodolomite (Ca(Fe _m Mg _n)(CO ₃) ₂)	$\begin{aligned} &CaCO_3 + CO_2 + H_2O \! \to \! Ca^{2+} + 2HCO_3^- \\ &CaMg(CO_3)_2 + 2CO_2 + 2H_2O \! \to \! Ca^{2+} + Mg^{2+} + 4HCO_3^- \\ &2KAlSi_3O_8 + 2CO_2 + 11H_2O \! \to \! Al_2Si_2O_5(OH)_4 \!\downarrow + 2HCO_3^- + 2K^+ + 4H_4SiO_4 \\ &2NaAlSi_3O_8 + 2CO_2 + 11H_2O \! \to \! Al_2Si_2O_5(OH)_4 \!\downarrow + 2HCO_3^- + 2Na^+ + 4H_4SiO_4 \\ &\mathit{Ca(Fe_mMg_n)(CO_3)_2 + 2CO_2 + 2H_2O \! \to \! 4HCO_3^- + Ca^{2+} + nMg^{2+} + mFe^{2+} \end{aligned}$	/ / Kaolinite (Al ₂ Si ₂ O ₅ (OH) ₄) Kaolinite (Al ₂ Si ₂ O ₅ (OH) ₄) /

3.1.3. Corrosion of pure minerals

The mass of the mineral powder sample was measured after dried within the specified sampling intervals. Then, the dissolution rate (Eq. (2)) for each mineral is calculated across various reaction durations. The results are presented in Fig. 4.

$$R_{\rm d} = (m_1 - m_2) / m_1 \tag{2}$$

where R_d is the dissolution rate, %; m_1 is the initial mass of pure mineral, mg; m_2 is the pure mineral mass after dissolution, mg.

The dissolution rate of calcite quickly rose to 0.46% within the initial 40 h and ultimately reached 0.51%. Dolomite reaction primarily occurred in the initial stage, with the rate swiftly increasing to 0.29% within the first 5 h and ultimately reaching 0.41%. Potassium feldspar and albite exhibit slow dissolution rates at 0.22% and 0.16%, respectively. Ferrodolomite demonstrates an extremely low dissolution rate, measuring only 0.04%. Under experimental conditions, calcite and dolomite readily undergo corrosion reactions with carbonic acid, displaying a strong sensitivity to it. Rapid mineral dissolution leads to the formation of soluble matter, causing a decrease in mineral mass and an increase in corrosion rate. The dissolution rate of pure minerals generally exhibits an increasing trend over time, signifying complete exposure to carbonic acid. The mineral corrosion reaction persists, constituting a prolonged chemical reaction process. During the corrosion reaction, the dissolution rates stabilized at 40 h for calcite, potassium feldspar and albite, and 15 h for dolomite, respectively. The kaolinite generated by the reaction ceased participation, leading to the passivation of the original mineral surface. Consequently, the concentrations of ions in solution no longer experienced a rapid increase.

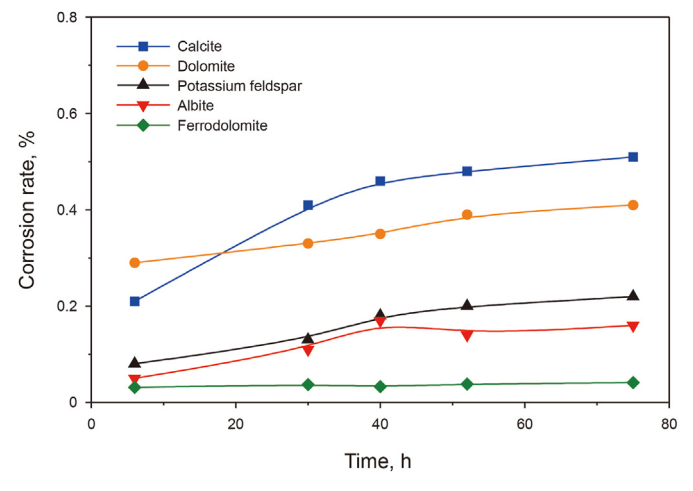


Fig. 4. Corrosion rate of pure minerals with carbonic acid.

3.2. Solution ion evolution during carbonic acid corrosion

3.2.1. Ionic variation during core dissolution

During the carbonic acid—core corrosion experiment, the introduction of a saturated simulated CO_2 solution into the core initiates multiple reactions within core pores. Subsequently, the reaction solution was collected at the predetermined reaction time, and its ionic composition and content were analyzed using an inductively coupled plasma mass spectrometer. Fig. 5 illustrates the temporal variations in concentrations of Ca^{2+} , Mg^{2+} , Na^+ , K^+ , and Fe^{2+} .

Since the dissolved products of calcite and dolomite both contain Ca^{2+} , Ca^{2+} is selected as the representative ion of calcite during its dissolution process, the influence of Ca^{2+} produced by dolomite should be excluded. Since the reaction of carbonic acid—dolomite generates the same amount of Ca^{2+} and Mg^{2+} , the Ca^{2+} concentration is modified by referring to Eq. (3). The result is shown in Fig. 6

$$C_{Ca^{2+}} = C_{t(Ca^{2+})} - C_{t(Mg^{2+})}$$
(3)

where $C_{\text{Ca}^{2+}}$ is the Ca^{2+} concentration from the dissolution of calcite, mg/L; $C_{t(\text{Ca}^{2+})}$ is the total concentration of Ca^{2+} in the effluent at any time t, mg/L; $C_{t(\text{Mg}^{2+})}$ is the total concentration of Mg^{2+} in the effluent at any time t, mg/L.

Notably, among the core components, calcite and dolomite exhibit heightened corrosion sensitivity, leading to elevated ion concentrations during the multiple-phase reaction. In the initial stages of the reaction, the Ca²⁺ concentration sharply rose to 230.3 mg/L after 5 h of corrosion, followed by a rapid decline from 161.5 to 33.4 mg/L between 5 and 16 h. Subsequently, in the later stages of the reaction, the Ca²⁺ concentration gradually decreased, ultimately stabilizing at 72.9 mg/L. Calcite exhibits a high sensitivity to dissolution. Upon injecting carbonic acid into the core, rapid corrosion reactions occurred upon contact with calcite, yielding a substantial amount of Ca²⁺. Ca²⁺ became enriched on the surface of calcite and was carried out of the core with the solution. resulting in elevated ion concentrations during the initial stages of the reaction. Subsequently, during the later stages of the reaction. the Ca²⁺ concentration gradually decreased. The diminished content of calcite, limited contact with carbonic acid during this period, and significant consumption in the early corrosion reaction contributed to the reduction of calcite in the later stages. Simultaneously, mineral precipitation resulting from the corrosion reaction might adhere to the mineral surface, diminishing the reaction area and causing a decrease in Ca²⁺ concentration. Initially, the Mg²⁺ concentration was high at the onset of the corrosion reaction. However, as the corrosion reaction progressed, the Mg^{2+} concentration exhibited a consistent upward trend, ultimately reaching 74.4 mg/L. Given that both calcite and dolomite yield Ca²⁴ following carbonic acid dissolution, the Ca²⁺ concentration is notably higher than that of Mg²⁺ in the initial stages of the reaction. Potassium feldspar, albite, and ferrodolomite exhibited low

Potassium feldspar, albite, and ferrodolomite exhibited low dissolution sensitivity, resulting in correspondingly low

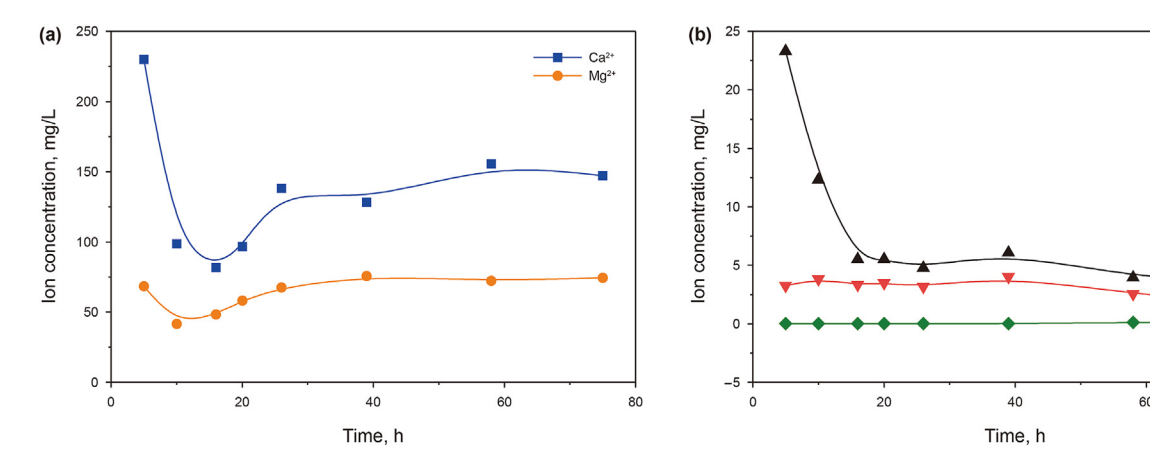


Fig. 5. Variations in ion concentrations during carbonic acid corrosion.

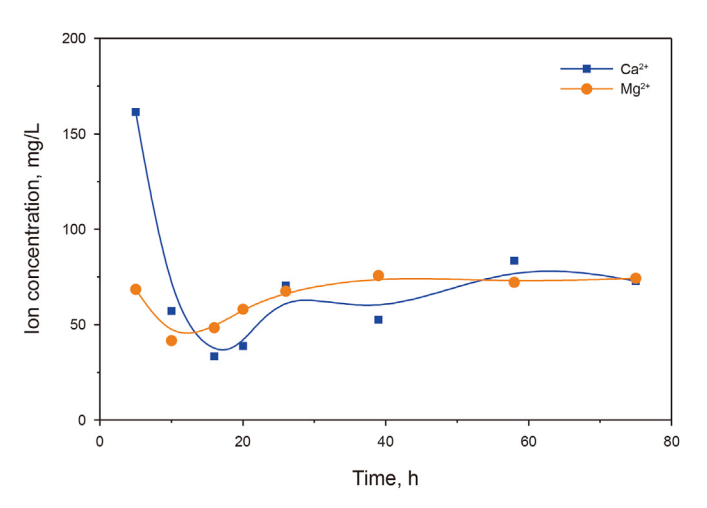


Fig. 6. Variations in concentrations of Ca^{2+} and Mg^{2+} in the reaction effluent after calibration.

characteristic ion concentrations. Initially, the K⁺ concentration rose during the initial stages of the reaction, subsequently decreasing from 23.3 to 5.1 mg/L within 5-20 h before exhibiting a gradual overall decline, stabilizing at a final concentration of 3.7 mg/L. As potassium feldspar undergone dissolution, it gradually depleted, forming kaolinite. This process led to a reduction in the contact area between fresh potassium feldspar and carbonic acid, consequently decreasing the corrosion rate. The overall Na⁺ concentration exhibited a gradual decline, ranging from 1 to 4 mg/L, eventually stabilizing at approximately 1.8 mg/L. Albite demonstrates general sensitivity to corrosion, persisting in corrosion by carbonic acid. This ongoing process resulted in a gradual decrease in Na⁺ concentration as its own quantity diminished. Throughout the corrosion reaction process, the Fe²⁺ concentration consistently remained below 0.15 mg/L. Ferrodolomite exhibited weak sensitivity to corrosion, proving resistant to corrosion with carbonic acid.

3.2.2. Ionic variation during pure mineral dissolution

Throughout the carbonic acid—pure mineral corrosion experiment, carbonic acid remained consistently saturated, ensuring continuous interaction with the pure mineral. At each sampling interval, the dissolution solution from the pure mineral, corresponding to the reaction container, was collected. An inductively coupled plasma mass spectrometer was employed to test and analyze the composition and content of characteristic ions in the pure mineral

dissolution solution. The results are presented in Fig. 7.

Calcite and dolomite exhibit higher dissolution sensitivity in the carbonic acid-pure mineral corrosion experiment, aligning with findings from the carbonic acid-core corrosion experiment. In the initial stages of the reaction, the Ca²⁺ concentration in the calcite solution and the Mg²⁺ concentration in the dolomite solution experienced rapid increases, reaching 238.4 and 99.2 mg/L, respectively, after 6 h of dissolution. Subsequently, their concentrations increased gradually and stabilized as the corrosion reaction progressed, reaching 271.4 and 145.7 mg/L, respectively. The corrosion reaction of calcite and dolomite with carbonic acid primarily transpired in the early stages, characterized by rapid and substantial dissolution of both minerals. The Ca²⁺ concentration surpassed that of Mg²⁺, signifying a greater degree of corrosion reaction between calcite and dolomite with carbonic acid. This implies a higher sensitivity to dissolution, with calcite exhibiting the strongest sensitivity.

Potassium feldspar, albite, and ferrodolomite exhibit low corrosion sensitivity. Overall, the concentrations of K⁺ and Na⁺ gradually increased over time, eventually stabilizing at 16.1 and 9.5 mg/L, respectively. In contrast, the concentration of Fe²⁺ consistently remained at 0.4 mg/L. The low concentrations of K⁺ and Na⁺ suggest a limited degree of corrosion reaction between potassium feldspar and albite and carbonic acid, resulting in a moderate sensitivity to dissolution. The consistently low concentration of Fe²⁺ indicates that ferrodolomite resists corrosion with carbonic acid, showcasing a very weak sensitivity to dissolution.

The corrosion sensitivity of each pure mineral in the carbonic acid—pure mineral corrosion experiment aligns with the findings of the core experiment. The order of dissolution sensitivity is calcite > dolomite > potassium feldspar > albite > ferrodolomite. This correspondence underscores a high correlation between the carbonic acid corrosion with pure mineral and core samples. Consequently, establishing a correlation in the corrosion kinetics of the two is deemed essential.

3.2.3. Analysis of passivation mechanism in the process of corrosion

The experimental results reveal variations in the sensitivity of different minerals to carbonic acid. Considering the diverse structures of these minerals, their dissolution characteristics also differ accordingly. The corrosion reaction within the core can be delineated into three distinct stages. Initially, when the mineral encounters carbonic acid, corrosion of the mineral itself ensues. As the reaction time progresses and the injected liquid erodes, the pure mineral is gradually stripped away. The injected fluid, as it traverses the narrow throat, is susceptible to deposition and blockage due to

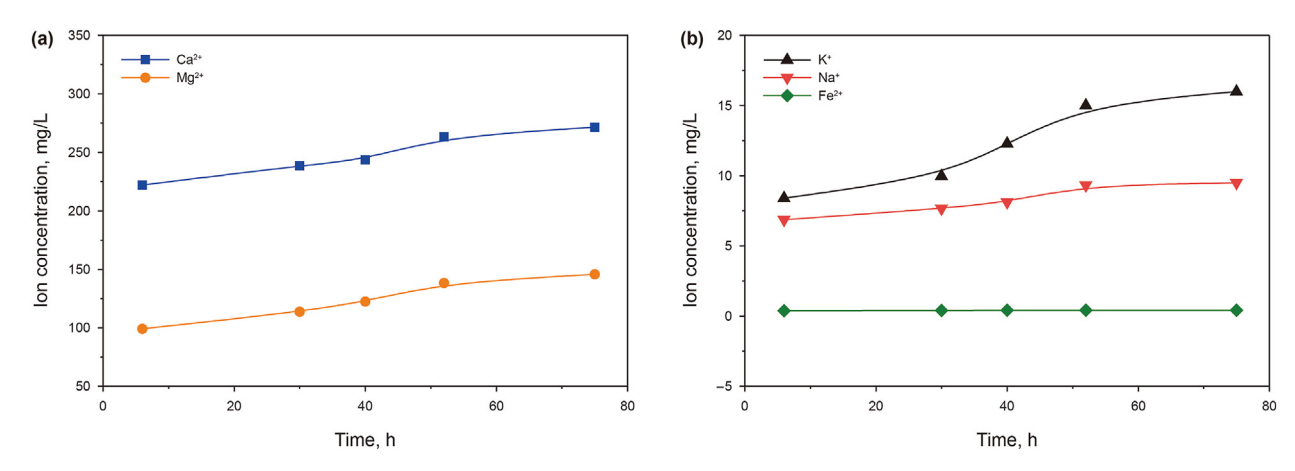


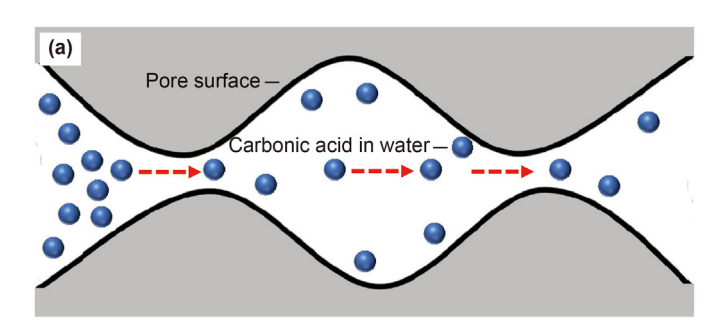
Fig. 7. Variations in ion concentrations in the pure mineral solution during corrosion.

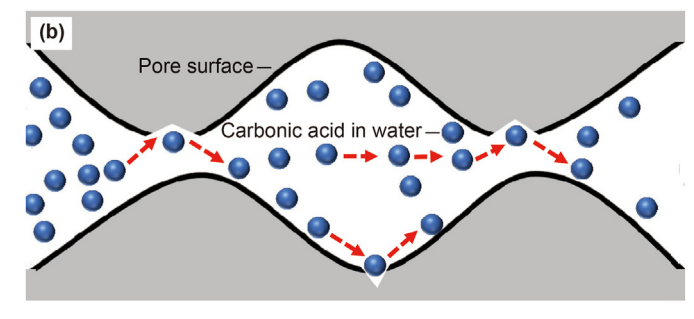
the constrained passage. The illustration of these three stages is presented in Fig. 8.

3.3. Kinetics of carbonic acid—pure mineral corrosion

3.3.1. Kinetics of the carbonic acid—pure mineral corrosion reaction

The rate of carbonic acid reaction with pure minerals can be





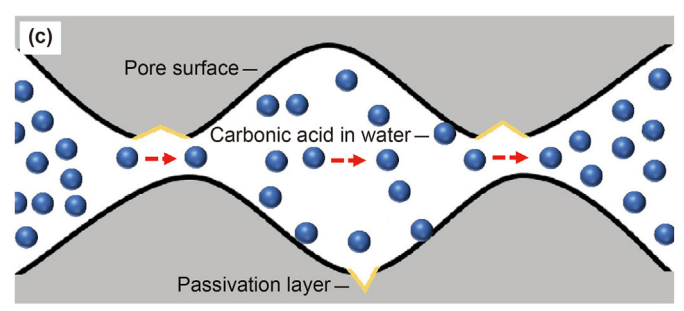


Fig. 8. Schematic diagram of passivation reaction in pure mineral. Carbonic acid enters into the pore space (a) and dissolves minerals in pore surface (b); (c) Undissolved reaction production deposits and forms a passivation layer.

quantified by the reduction in the carbonic acid concentration in the solution over time. According to the law of mass action, which states that under constant temperature and pressure, the chemical reaction rate is proportional to the product of the relevant powers of the reactant concentrations, and the reaction rate between carbonic acid and a pure mineral can be determined. Given the complexity of carbonic acid—pure mineral corrosion reactions involving multiple phases, the concentration of pure mineral reactants can be considered a constant. Consequently, the reaction rate between carbonic acid and a pure mineral can be expressed as Eq. (4) (Lund et al., 1975):

$$J = -\frac{\partial C}{\partial t} = KC^m \tag{4}$$

where J is the reaction rate, indicating the decrease in the carbonic acid concentration per unit time, $(\text{mol/L}) \cdot \text{s}^{-1}$; C is the carbonic acid concentration of the acid solution at time t, mol/L; K is the reaction rate constant, $(\text{mol/L})^{1-m} \cdot \text{s}^{-1}$; m is the reaction order; and t is the reaction time, t.

In this experiment, which was conducted under specific temperature and pressure conditions, the concentration of carbonic acid in the solution remained constant since the liquid—solid ratio is extremely high in the piston accumulator. Consequently, the change in the ion concentration of the solution was employed to characterize the carbonic acid—pure mineral corrosion reaction rate. Thus, the reaction rate in this study can be given by Eq. (5):

$$J = \frac{\partial C_1}{\partial t} = KC_1^m \tag{5}$$

where J is the reaction rate, representing the increase in the reactant ion concentration per unit time, (mol/L)·s⁻¹; C_1 is the concentration of produced ions in the solution at time t, mol/L.

When the logarithm of the produced ion concentration is taken as the horizontal coordinate and the logarithm of the reaction rate is taken as the vertical coordinate, as in Eq. (6), the slope is m, and the intercept is lgK. This curve was drawn according to the results of the carbon dioxide dissolution experiment, both the reaction rate and concentrations in carbonic acid—pure mineral corrosion reactions were calculated. Then, the reaction parameters of carbonic acid—pure mineral corrosion were obtained.

$$\lg J = \lg K + m \lg C_1 \tag{6}$$

3.3.2. Kinetic equation of the carbonic acid—pure mineral corrosion reaction

At the designated reaction time, the reaction liquid resulting from the interaction of carbonic acid and a pure mineral was collected. The composition and contents of characteristic ions in the solution were then measured and analyzed via an inductively coupled plasma mass spectrometer. The correlation between the concentrations of corresponding ions in the solution and time can be determined. The reaction rates at various time intervals were calculated subsequently, and both lg/ and lg/ were taken to generate Fig. 9.

In Fig. 9, the relationship between the reaction rate and the calcium concentration indicates that the reaction behavior can be divided into two stages. By employing the least squares method for linear regression, the kinetic parameters for the carbonic acid—pure mineral reaction in the two stages can be obtained as follows.

In the rapid reaction stage, the reaction rate constant $K = 10^{-51.46} = 3.47 \times 10^{-52}$, and the reaction order m = -19.89, as

shown in Eq. (7).

$$I_1 = 3.47 \times 10^{-52} C^{-19.89} \tag{7}$$

In the slow reaction stage, the reaction rate constant $K = 10^{-16.98} = 1.05 \times 10^{-17}$, and the reaction order m = -4.34, as shown in Eq. (8).

$$I_2 = 1.05 \times 10^{-17} C^{-4.34}$$
 (8)

By calculating the kinetic processes of other mineral reactions, the kinetic parameters for the two stages can be obtained, as shown in Table 2.

3.4. Mineral dissolution correlation of cores and pure minerals

3.4.1. Correlation of sample mass

Owing to their high availability, low cost, high purity, simple operation in corrosion experiments with pure minerals, acquisition

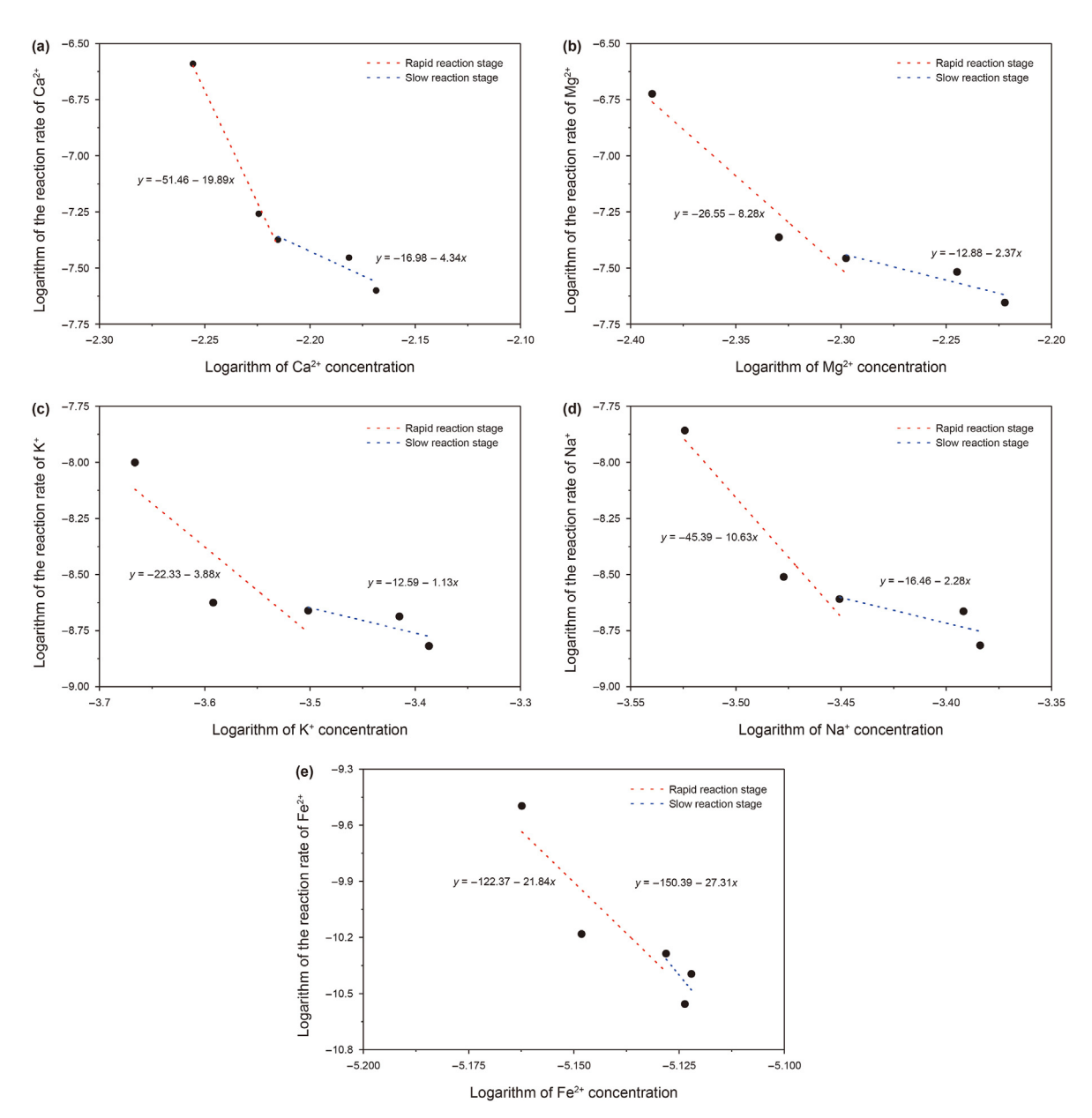


Fig. 9. Relationships between reaction rates of various ions and their concentrations during the reaction.

Table 2Kinetic parameters at different stages of the reaction.

Mineral	Featured ion	Reaction stage	Equation	т	K , $(\text{mol/L})^{1-m} \cdot \text{s}^{-1}$
Calcite	Ca ²⁺	Rapid	$J_1 = K_1 C^{m_1}$	-19.89	3.47×10^{-52}
		Slow	$J_2 = K_2 C^{m_2}$	-4.34	1.05×10^{-17}
Dolomite	${\sf Mg}^{2+}$	Rapid	$J_1 = K_1 C^{m_1}$	-8.28	2.82×10^{-27}
	_	Slow	$J_2 = K_2 C^{m_2}$	-2.37	1.32×10^{-13}
Potassium feldspar	K^+	Rapid	$J_1 = K_1 C^{m_1}$	-3.88	4.68×10^{-23}
		Slow	$J_2 = K_2 C^{m_2}$	-1.13	2.57×10^{-13}
Albite	Na ⁺	Rapid	$J_1 = K_1 C^{m_1}$	-10.63	4.07×10^{-46}
		Slow	$J_2 = K_2 C^{m_2}$	-2.28	3.47×10^{-17}
Ferrodolomite	Fe ²⁺	Rapid	$J_1 = K_1 C^{m_1}$	-21.84	4.30×10^{-123}
		Slow	$J_2 = K_2 C^{m_2}$	-27.31	4.10×10^{-151}

of reaction parameters from carbonic acid—pure minerals is much easier than that with core samples. However, due to the geological sediment and heterogeneity of the reservoir, the corrosion reactions between different reservoirs and carbonic acid can be significantly different. The application of corrosion reaction parameters obtained from pure minerals, in conjunction with the quantitative relationship between a core and the corrosion behavior of pure minerals, allows a reasonable prediction of the corrosion between reservoirs and carbonic acid. This approach facilitates quantitative evaluation of the corrosion behavior in the reservoir.

After both core samples and pure minerals were subjected to a 75-h corrosion reaction with carbonic acid, the mass changes for different minerals in the cores and the pure minerals were calculated, respectively. This allowed a relationship between the mass changes in cores and single minerals to be established, as illustrated in Fig. 10. The mass change of ferrodolomite in the pure mineral and core is the smallest, which indicates that its reactivity is the lowest. In contrast, calcite and dolomite, which have high mass changes in both the pure minerals and cores, exhibit good reactivity and they are the main participants in the corrosion reactions.

3.4.2. Correlation of mineral reaction rates

After both core samples and pure minerals were subjected to a 75-h corrosion reaction with carbonic acid, the ion concentrations stabilized. At this point, the average reaction rates for different minerals in the cores and the pure minerals were calculated. This facilitated the establishment of a relationship between the ion

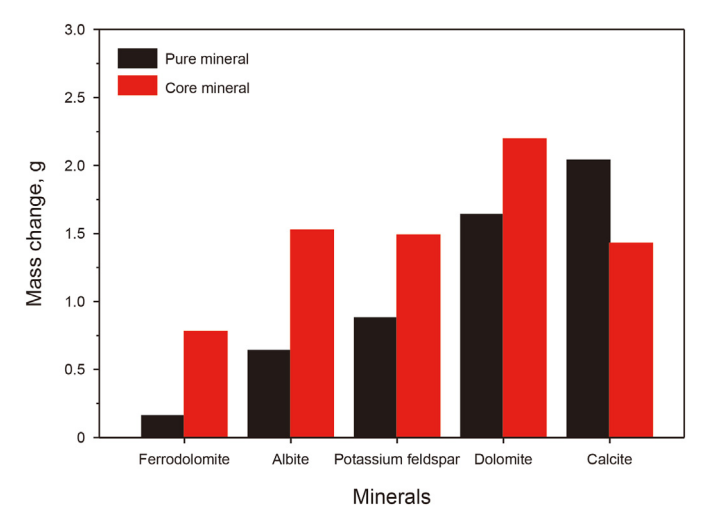


Fig. 10. Mineral mass variations in core and pure mineral after corrosion.

reaction rates in the cores and pure minerals, as illustrated in Fig. 11.

The experimental results indicate that minerals with greater sensitivity to corrosion exhibit faster reaction rates and that the ratio of characteristic ions is lower when the concentrations in dissolution solutions of pure minerals and cores stabilize. The sensitivity of minerals to carbonic acid is influenced primarily by their crystal structure. The greater sensitivity of minerals to carbonic acid implies a reduced influence from external factors such as the pore structure of the core, reaction contact area, and carbonic acid concentration on the mineral surface. This, in turn, results in the corrosion reaction degrees of pure minerals and cores with carbonic acid being more similar.

Limestone has the highest sensitivity to carbonic acid corrosion, with a dissolution rate of $1.13\times10^{-8}~(\text{mol/L})\cdot\text{s}^{-1}$ in the core samples. Calcite shows a relatively high sensitivity, attaining a maximum dissolution rate in the cores of $6.75\times10^{-9}~(\text{mol/L})\cdot\text{s}^{-1}$. Potassium feldspar and sodium feldspar demonstrate moderate sensitivity to carbonic acid corrosion, with dissolution rates of 3.51×10^{-10} and $2.9\times10^{-10}~(\text{mol/L})\cdot\text{s}^{-1}$, respectively, in the core samples. Ferrodolomite is the least sensitive to dissolution, with the dissolution rate in the core samples falling below $3.98\times10^{-12}~(\text{mol/L})\cdot\text{s}^{-1}$.

3.4.3. Correlation of ion concentrations

The concentration of ions in the dissolution solution of pure minerals is greater than that of the same ions in the dissolution solution of core samples. This difference can be attributed to the larger specific surface area of powdered pure minerals. Influenced by the pore structure of the core, minerals within the core may not achieve full contact with carbonic acid. Additionally, corrosion

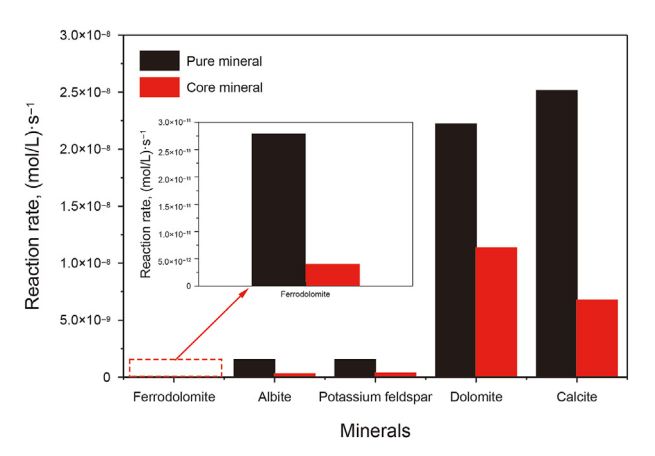


Fig. 11. Reaction rates in core and pure minerals.

reactions within the core are more complex, and secondary mineral precipitates may adhere to pore surfaces, further reducing the contact area between minerals and carbonic acid. Consequently, the concentration of ions in the dissolution solution of pure minerals surpasses that of the same ions in the dissolution solution of core samples, indicating a more thorough corrosion reaction between pure minerals and carbonic acid.

After 75 h of the corrosion reaction, both the core samples and pure minerals undergo comprehensive corrosion reactions with carbonic acid, leading to stabilization of the characteristic ion concentrations in the dissolution solutions. By analyzing the change in the mineral content and ion concentrations in dissolution solutions of pure minerals and core samples, respectively, the experimental results are presented in Table 3.

4. Discussion

4.1. Implications of carbonic acid reactions with cores and pure minerals

The core corrosion experiment involves a prolonged duration and a complex process. The experimental results closely align with the actual conditions of the target block. However, these results exhibit regional limitations, since each block has their unique properties, such as different mineral contents, pore structure, water salinity, temperature, pressure, etc. Conversely, the pure mineral corrosion experiment is characterized by a brief duration and a straightforward process. However, its results lack specificity. Therefore, we aim to integrate these two methods to derive a more effective and expeditious approach for evaluating the carbonic acid—core reactions in certain reservoir conditions, as shown in Fig. 12. This comprehensive method not only yields more practical experimental results with real core samples but also can be completed in a shorter timeframe, providing a viable path for rapid assessment of carbonic acid—core reactions.

The reaction kinetics formulas for different minerals obtained

from pure mineral experiments, combined with the ion concentration ratios obtained from stable moments in core experiments, can be used to derive a relationship formula for the ion concentrations in cores at any given moment. This provides an effective quantitative method for rapidly evaluating of carbonic acid—core reactions, as shown in Eq. (9).

$$\begin{cases} C_{m-a_1} = C_0 + J_1 t \\ C_{m-a_2} = C_0 + J_1 t + J_2 (t - t_1) \end{cases}$$

$$\begin{cases} C_{m-b_1} = C_0 + J_1 t \\ C_{m-b_2} = C_0 + J_1 t + J_2 (t - t_1) \end{cases}$$
...
$$\begin{cases} C_{m-i_1} = C_0 + J_1 t \\ C_{m-i_2} = C_0 + J_1 t + J_2 (t - t_1) \end{cases}$$

$$\begin{cases} C_{m-i_2} = C_0 + J_1 t + J_2 (t - t_1) \\ C_{m-i_2} = C_0 + J_1 t + J_2 (t - t_1) \end{cases}$$

$$\begin{cases} C_{c_1} = \alpha (n_1 C_{m-a_1} + n_2 C_{m-b_1} + \dots + n_i C_{m-i_1}) \\ C_{c_2} = \alpha (n_1 C_{m-a_2} + n_2 C_{m-b_2} + \dots + n_i C_{m-i_2}) \end{cases}$$

where C_{m-a_1} is the concentration of pure mineral a at time t in the rapid reaction stage, mol/L; C_{m-a_2} is the concentration of pure mineral a at time t in the slow reaction stage, mol/L; C_{m-b_1} is the concentration of pure mineral b at time t in the rapid reaction stage, mol/L; C_{m-b_2} is the concentration of pure mineral b at time t in the slow reaction stage, mol/L; C_{m-i_1} is the concentration of pure mineral i at time t in the rapid reaction stage, mol/L; C_{m-i_2} is the concentration of pure mineral i at time i in the slow reaction stage, mol/L; i is the rapid reaction rate, (mol/L)·s⁻¹; i is the slow reaction rate, (mol/L)·s⁻¹; i is the ion concentration ratio, dimensionless; i is the reaction time, i is the end time of the rapid reaction stage, i is the rapid reaction stage, i is the end time of the rapid reaction stage, i is the reaction time, i is the end time of the rapid reaction stage, i is the reaction time, i is the end time of the rapid reaction stage, i is the reaction time, i is the end time of the rapid reaction stage, i is the reaction time, i is the end time of the rapid reaction stage, i is the reaction time, i is the end time of the rapid reaction stage, i is the reaction time, i is the end time of the rapid reaction stage, i is the reaction time, i is the end time i the end time i the reaction stage, i is the reaction time, i is the end time i the rapid reaction stage, i is the reaction time, i the rapid reaction stage, i is the reaction time, i is the rapid reaction time, i the rapid reaction time i the rapid reaction tim

Table 3 Ion concentrations in the core and mineral dissolution solutions at the final time.

Mineral	Featured ion	lon concentration from pure mineral corrosion, mol/L	Ion concentration from core corrosion, mol/L	Ratio
Calcite	Ca ²⁺	0.0068	0.0018	3.77
Dolomite	Mg^{2+}	0.0059	0.0031	1.90
Potassium feldspar	K^+	0.00041	0.000095	4.32
Albite	Na ⁺	0.00041	0.000078	5.25
Ferrodolomite	Fe ²⁺	0.0000072	0.0000011	6.54

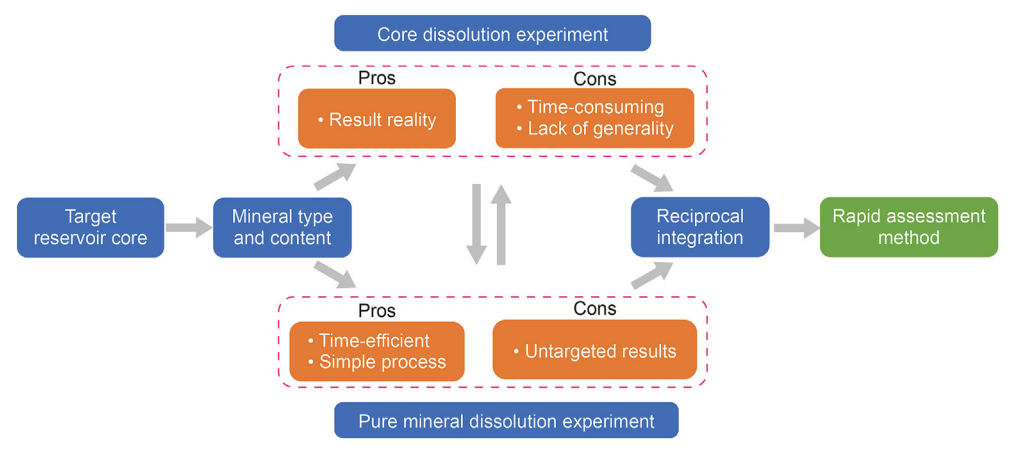


Fig. 12. Flowchart of rapid assessment of carbonic acid—core reactions.

represent the mass fractions of pure minerals a, b, ..., i, dimensionless; C_{c_1} is the total ion concentration of the core in the rapid reaction stage, mol/L; and C_{c_2} is the total ion concentration of the core in the slow reaction stage, mol/L.

A comparison of the carbonic acid corrosion experiments with pure minerals and cores reveals that the reactions of a mineral in the core are correlated with those from same pure mineral. The dissolution behavior in reservoirs induced by CO_2 injection can be predicted to a certain extent through pure mineral experiments, which would be much simpler and easier.

4.2. Limitations

Owing to the variability in the reservoir mineral composition and the differences in the formation temperature and pressure conditions, the scope of this study is subject to certain limitations. The experimental results obtained in this study are specifically applicable to tight sandstone samples and to the experimental conditions employed in this study. Variations in oil—water saturation and distribution characteristics, mineral types and distributions, core samples with different porosities, and differences in the experimental temperature and pressure may lead to differences in the carbonic acid—mineral reaction behavior and reaction rates. Future research should consider these factors across different samples and environmental conditions to further validate and expand our findings.

5. Conclusions

In this study, the carbonic acid corrosion with core and pure minerals was investigated in detail. The mineral variation of tight rock and pure minerals throughout the corrosion process was clarified. Additionally, the ionic characterization in both corrosion solutions was analyzed. Furthermore, correlations between the rock and pure minerals were established. The main conclusions may be drawn as follows:

- (1) After carbonic acid corrosion, the calcite, dolomite, potassium feldspar, albite, and ferrodolomite in the core sample were consumed, and their contents were all decreased. However, the reaction produced additional quartz and clay, resulting in a slight increase in their contents.
- (2) When the corrosion was stabilized in the core solution, the concentrations of Ca²⁺ and Mg²⁺ in the core solution were 72.9 and 74.4 mg/L, respectively, which was 40.5–41.3 times higher than that of Na⁺. However, for the corrosion with pure minerals, the concentrations of divalent ions were much higher. They were 271.4 and 145.7 mg/L for Ca²⁺ and Mg²⁺, respectively.
- (3) During the carbonic acid—pure mineral corrosion reaction, distinct minerals exhibit similar variation characteristics of ion concentration. The kinetics of the carbonic acid corrosion reaction were determined with the corrosion reaction rate equation. The reaction rate constant and reaction orders between the rapid and slow reaction stage stages for each ion were calculated.
- (4) With the comparison of carbonic acid reaction with rock and pure mineral, their mass variation, corrosion rate of minerals, and ion concentration were used to generate a corresponding relationship between the two reactions.
- (5) The experiment of carbonic acid reaction with core samples takes a long time and the procedure is complicated. On the contrary, the experiment with pure minerals takes a shorter time and is easier to carry out. With the correlation between carbonic acid reaction with core and pure minerals, an

effective and rapid evaluation method with pure minerals for the carbonic acid—rock reaction is established. However, more experiments are expected to improve the application from mineral data to rock data.

CRediT authorship contribution statement

Yong-Peng Sun: Writing — review & editing, Funding acquisition, Data curation, Conceptualization. **Guo-Liang Li:** Writing — review & editing, Investigation, Data curation. **Si-Zhe Zeng:** Writing — review & editing. **Jia-Wei Liu:** Formal analysis, Conceptualization. **Xian-Fei Du:** Resources, Project administration, Formal analysis. **Cai-Li Dai:** Supervision, Funding acquisition.

Data availability

Data will be made available on request.

Declaration of competing interest

The authors declare that they have no known competing financial interests or personal relationships that could have appeared to influence the work reported in this paper.

Acknowledgements

The authors would like to acknowledge the National Natural Science Foundation of China (52474073, 52288101, 52120105007, 51804327), Shandong Provincial Natural Science Foundation (ZR2023ME016) and Climb Taishan Scholar Program in Shandong Province (tspd20230605).

References

- Cao, C., Song, Z., Shi, Y., et al., 2023. Study on CO₂ Huff-N-Puff enhanced recovery technology for Jimsar shale oil. Special Oil Gas Reservoirs 30 (3), 106–114. https://doi.org/10.3969/j.issn.1006-6535.2023.03.013 (in Chinese).
- Chen, J., Yang, R., Huang, Z., et al., 2023. Simulation study of supercritical carbon dioxide jet fracturing for carbonate geothermal reservoir based on fluid-thermo-mechanical coupling model. Pet. Sci. 20 (3), 1750–1767. https://doi.org/10.1016/j.petsci.2022.11.005.
- Eyinla, D.S., Leggett, S., Badrouchi, F., et al., 2023. A comprehensive review of the potential of rock properties alteration during CO₂ injection for EOR and storage. Fuel 353, 129219. https://doi.org/10.1016/j.fuel.2023.129219.
- Fuel 353, 129219. https://doi.org/10.1016/j.fuel.2023.129219.

 Fatah, A., Mahmud, H.B., Bennour, Z., et al., 2021. Effect of supercritical CO₂ treatment on physical properties and functional groups of shales. Fuel 303, 121310. https://doi.org/10.1016/j.fuel.2021.121310.
- Gholami, R., Raza, A.J.F., 2022. CO₂ sequestration in sandstone reservoirs: how does reactive flow alter trapping mechanisms? Fuel 324, 124781. https://doi.org/ 10.1016/j.fuel.2022.124781.
- Hematpur, H., Abdollahi, R., Rostami, S., et al., 2023. Review of underground hydrogen storage: concepts and challenges. Adv. Geo-Energy Res. 7 (2), 111–131. https://doi.org/10.46690/ager.2023.02.05.
- Jia, C.Q., Sepehrnoori, K., Zhang, H.Y., et al., 2022. Numerical investigation of fluid phase momentum transfer in carbonate acidizing. Pet. Sci. 19 (2), 639–650. https://doi.org/10.1016/j.petsci.2021.11.016.
- Kaszuba, J.P., Janecky, D.R., Snow, M.G., 2005. Experimental evaluation of mixed fluid reactions between supercritical carbon dioxide and NaCl brine: relevance to the integrity of a geologic carbon repository. Chem. Geol. 217 (3–4), 277–293. https://doi.org/10.1016/j.chemgeo.2004.12.014.
- Khather, M., Yekeen, N., Al-Yaseri, A., et al., 2022. The impact of wormhole generation in carbonate reservoirs on CO₂-WAG oil recovery. J. Petrol. Sci. Eng. 212, 110354. https://doi.org/10.1016/j.petrol.2022.110354.
- Li, N., Jin, Z., Zhang, S., et al., 2023. Micro-mechanical properties of shale due to water/supercritical carbon dioxide-rock interaction. Petrol. Explor. Dev. 50 (4), 872–882. https://doi.org/10.1016/S1876-3804(23)60445-8.
- Li, P., Yang, Y., Wang, M., et al., 2022. Study on the coal damage effects caused by the CO₂-alkaline water two-phase displacing gas and wetting coal. Fuel 310, 122305. https://doi.org/10.1016/j.fuel.2021.122305.
- Liang, Y., Chen, Q., Liao, Z., et al., 2021. Dissolution effect of carbonate minerals on shale pores and its significance: a case study on the Lower Silurian Longmaxi Formation shale in the eastern Sichuan Basin. Nat. Gas. Ind. 41 (1), 93–101. https://doi.org/10.3787/j.issn.1000-0976.2021.01.008 (in Chinese).

Liu, J., 2022. Progress and prospect of production profile testing technology for staged fracturing in horizontal wells. Special Oil Gas Reservoirs 29 (5), 1–8. https://doi.org/10.3969/j.issn.1006-6535.2022.05.001 (in Chinese).

- Liu, S., Jiao, K., Zhang, J., et al., 2021. Research progress on the pore characteristics of deep shale gas reservoirs: an example from the Lower Paleozoic marine shale in the Sichuan Basin. Nat. Gas. Ind. 41 (1), 29–41. https://doi.org/10.3787/ j.issn.1000-0976.2021.01.003 (in Chinese).
- Liu, X., Zhang, C., Nie, B., et al., 2022. Mechanical response and mineral dissolution of anthracite induced by supercritical CO₂ saturation: influence of saturation time. Fuel 319, 123759. https://doi.org/10.1016/j.fuel.2022.123759.
- Liu, Z., Zhou, Q., Cong, S., et al., 2023. Corrosion behavior of a new alumina-forming duplex stainless steel with different surface treatment in supercritical carbon dioxide. Surf. Coating. Technol. 466, 129619. https://doi.org/10.1016/j.surfcoat.2023.129619.
- Lu, Y., Liu, J., Tang, J., et al., 2022. Pore changes of slick water-containing shale under supercritical CO₂ treatment. Fuel 312, 122775. https://doi.org/10.1016/ifuel_2021122775
- Lund, K., Fogler, H., McCune, C., et al., 1975. Acidization-II. The dissolution of calcite in hydrochloric acid. Chem. Eng. Sci. 30, 825–835. https://doi.org/10.1016/ 0009-2509(75)80047-9.
- Memon, S., Feng, R., Ali, M., et al., 2022. Supercritical CO₂-shale interaction induced natural fracture closure: implications for scCO₂ hydraulic fracturing in shales. Fuel 313, 122682. https://doi.org/10.1016/j.fuel.2021.122682.
- Ozotta, O., Ostadhassan, M., Liu, K., et al., 2021. Reassessment of CO₂ sequestration in tight reservoirs and associated formations. J. Petrol. Sci. Eng. 206, 109071. https://doi.org/10.1016/j.petrol.2021.109071.
- Song, Y., Zou, Q., Su, E., et al., 2020. Changes in the microstructure of low-rank coal after supercritical CO₂ and water treatment. Fuel 279, 118493. https://doi.org/10.1016/j.fuel.2020.118493.
- Sun, Y., Dai, C., Yu, Z., et al., 2021. The carbonic acid-rock reaction in feldspar/dolomite-rich tight sand and its impact on CO₂-water relative permeability during geological carbon storage. Chem. Geol. 584, 120527. https://doi.org/10.1016/i.chemgeo.2021.120527.
- Talebi, A., Hasan-Zadeh, A., Kazemzadeh, Y., et al., 2022. A review on the application of carbonated water injection for EOR purposes: opportunities and challenges. J. Petrol. Sci. Eng. 214, 110481. https://doi.org/10.1016/j.petrol.2022.110481.
- Tang, H., Meng, Y., Li, Y., et al., 2006. Experimental research on chemical behavior of kaolinite acid. Nat. Gas. Ind. 26 (10), 111–113. https://doi.org/10.3321/j.issn: 1000-0976.2006.10.035 (in Chinese).
- Wang, F., Zhang, X., Wu, C., et al., 2023. Mechanism of supercritical CO₂ on the chemical structure and composition of high-rank coals with different damage

- degrees. Fuel 344, 128027. https://doi.org/10.1016/j.fuel.2023.128027.
- Wigand, M., Carey, J.W., Schütt, H., 2008. Geochemical effects of CO₂ sequestration in sandstones under simulated in situ conditions of deep saline aquifers. Appl. Geochem. 23, 2735–2745. https://doi.org/10.1016/j.apgeochem.2008.06.006.
- Wu, D., Zhai, W., Liu, X., et al., 2023. The permeability of shale exposed to supercritical carbon dioxide. Sci. Rep. 13 (1), 6734. https://doi.org/10.1038/s41598-023-33702-1.
- Xu, L., Yue, Y., Chen, Y., et al., 2023. Effect of supercritical CO_2 on limestone's pore structure based on NMR and SEM. Petrol. Sci. Technol. 41 (15), 1510–1525. https://doi.org/10.1080/10916466.2022.2093368.
- Yan, W., Wei, H.-G., Muchiri, N.D., et al., 2023. Degradation of chemical and mechanical properties of cements with different formulations in CO₂-containing HTHP downhole environment. Pet. Sci. 20 (2), 1119–1128. https://doi.org/10.1016/j.petsci.2023.03.012.
- Yang, K., Zhou, J., Xian, X., et al., 2024. Changes of wettability of shale exposed to supercritical CO₂-water and its alteration mechanism: implication for CO₂ geosequestration. Fuel 357, 129942. https://doi.org/10.1016/j.fuel.2023.129942.
- Yang, Y., Horne, R.N., Cai, J., et al., 2023. Recent advances on fluid flow in porous media using digital core analysis technology. Adv. Geo-Energy Res. 9 (2), 71–75. https://doi.org/10.46690/ager.2023.08.01.
- Zhang, G., Ranjith, P., Wu, B., et al., 2019. Synchrotron X-ray tomographic characterization of microstructural evolution in coal due to supercritical CO₂ injection at in-situ conditions. Fuel 255, 115696. https://doi.org/10.1016/ifuel.2019.115696.
- Zhao, L., Jiang, E., Wang, S., et al., 2021. Effect of carbon dioxide injection on mineral and pore structure of low permeability reservoirs. Oilfield Chem. 38 (4), 659–664. https://doi.org/10.19346/j.cnki.1000-4092.2021.04.015 (in Chinese).
- Zhao, W., Zhu, R., Zhang, J., et al., 2023. Classification, exploration and development status and development trend of continental shale oil in China. China Petrol. Exploration 28 (4), 1–13. https://doi.org/10.3969/j.issn.1672-7703.2023.04.001 (in Chinese).
- Zhou, C., Remoroza, A.I., Shah, K., et al., 2016. Experimental study of static and dynamic interactions between supercritical CO₂/water and Australian granites. Geothermics 64, 246–261. https://doi.org/10.1016/ji.geothermics.2016.05.007.
- Zhou, J., Yang, K., Zhou, L., et al., 2021. Microstructure and mechanical properties alterations in shale treated via CO₂/CO₂-water exposure. J. Petrol. Sci. Eng. 196, 108088. https://doi.org/10.1016/j.petrol.2020.108088.
- Zou, S., Li, Y., Li, S., 2021. Influence of CO₂ pre-injection on fracture morphology and the petrophysical properties in shale fracturing. Nat. Gas. Ind. 41 (10), 83–94. https://doi.org/10.3787/j.issn.1000-0976.2021.10.009 (in Chinese).